Efficient Terahertz Generation via GaAs Hybrid Ridge Waveguides

Jialin Mei, Kai Zhong, Jiaming Xu, Degang Xu, Wei Shi, and Jianquan Yao

***Abstract*— As a common semiconductor material with high performance in the terahertz band, GaAs is hardly employed in second-order nonlinear frequency conversion (NFC) directly due to its isotropy. Although thin waveguides can break the symmetry and induce birefringence for phase matching (PM), more research seems to be needed with GaAs-based structures. In this paper, a category of ridge waveguide is demonstrated with a hybrid structure composed of GaAs and SiN in different sizes. By using the difference frequency generation (DFG) technique with 2 μm and 10 μm pump lasers, simulations suggest that the hybrid waveguides are able to generate continuous-wave (CW) monochromatic terahertz waves from 1.59 THz to 2.66 THz. The output power reach 56.16 μW, corresponding to a conversion efficiency of 5.62×10^{-5} W^{-1}, which is much higher than that using bulk GaAs crystals. Such integrated hybrid waveguides have great potential in efficient on-chip terahertz systems.**

***Index Terms*— Difference frequency generation (DFG), gallium arsenide (GaAs), ridge waveguides, terahertz waves.**

I. Introduction

DIFFERENCE frequency generation (DFG) plays a critical role in room-temperature monochromatic terahertz (THz) sources, which occupies a special status in the electromagnetic spectrum for their unique characteristics and great practical applications such as spectroscopy and bioimaging [1], [2]. Conventional nonlinear materials include birefringent crystals (such as GaSe, GaP, $ZnGeP_2$), organic crystals (such as DAST, DSTMS, and OH1), and artificially processed crystals (such as periodically poled $LiNbO_3$, and periodically inverted GaAs and GaP) using quasi-phase matching (QPM) [3], [4]. However, these crystals are not practical for compact systems, especially for on-chip applications, due to their disadvantages of bulky size, growth difficulty and inefficiency.

Over the past decade, a variety of integrated waveguides have been studied to achieve on-chip second-order nonlinear frequency conversion (NFC). Silicon on insulator (SOI) is an ideal platform for integrated optics with the merits of compatibility and low price, but the second-order nonlinear susceptibility of silicon is difficult to be exploited restricted by its centrosymmetric nature. The material symmetry of silicon-based waveguides can be broken by causing strain in the structures, and extensive investigations have shown the ability of NFC on SOI platforms [5], [6]. Nevertheless, the induced second-order nonlinear susceptibility is still very low [5]. Saito *et al*. made efforts on GaP-based waveguides to generate terahertz waves by DFG, and an output power of 0.66 mW was achieved at 5.93 THz with a conversion efficiency of 6.6×10^{-4} W^{-1} [7]. However, GaP is expensive and its absorption coefficient is relatively high among the infrared nonlinear materials, limiting its potential in improving the performance for terahertz generation. Waveguides based on $LiNbO_3$ have also drawn much attention, however, limited by its strong absorption, silicon-prism arrays are needed to extract the terahertz waves, resulting complexity to the systems [8].

GaAs has a large nonlinear susceptibility, a wide infrared transmission band, and low absorption coefficients in the terahertz range [9]. Besides, as a common semiconductor material in integrated optics, the cost of GaAs is very low with well-developed production techniques. Furthermore, its isotropic optical properties (e.g., refractive index) vanish when it is fabricated into waveguides with induced waveguide dispersion, allowing phase matching (PM) in a collinear configuration [10], [11]. Among all the integrated waveguide structures, a planar waveguide is easy to fabricate, but its ability to confine the lateral electric field is weak. The diversity of planar waveguides is also limited as only the thickness is variable. A strained waveguide, which usually combines with some other materials or configurations, has a complex manufacturing process, and the core region (usually several microns) is too small to confine the electric field of terahertz waves. As a result, the terahertz wave can penetrate into the surrounding materials, leading to a large propagation loss [6], [7], [12]. A slot waveguide in sub-wavelength scale demonstrates strong optical confinement to facilitate NFC efficiency but the fabrication is also complicated, which requires several etching and bonding processes [13]. Generally, a ridge waveguide is the best choice with flexible designs and simple fabrication. However, GaAs-based ridge waveguides, which should be a promising scheme, have not yet been investigated in terahertz generation through DFG.

In this paper, a practical GaAs/SiN composite ridge waveguide structure is proposed and theoretically studied for the generation of terahertz waves. The bottom SiN layer can be

Manuscript received April 13, 2019; revised June 14, 2019; accepted September 16, 2019. Date of publication September 23, 2019; date of current version October 1, 2019. This work was supported in part by the National Natural Science Foundation of China (NSFC) under Grant 61675146, in part by the Natural Science Foundation of Tianjin City under Grant 18JCYBJC16700, and in part by the Scholarship from the China Scholarship Council under Grant 201706250058. *(Corresponding author: Kai Zhong.)*

J. Mei is with the School of Precision Instruments and Optoelectronics Engineering, Tianjin University, Tianjin 300072, China, with the Key Laboratory of Opto-Electronic Information Technology, Ministry of Education (Tianjin University), Tianjin 300072, China, and also with the Department of Electrical and Computer Engineering, The University of Texas at Austin, Austin, TX 78712 USA (e-mail: meijialin@tju.edu.cn).

K. Zhong, D. Xu, W. Shi, and J. Yao are with the School of Precision Instruments and Optoelectronics Engineering, Tianjin University, Tianjin 300072, China, and also with the Key Laboratory of Opto-Electronic Information Technology, Ministry of Education (Tianjin University), Tianjin 300072, China (e-mail: zhongkai@tju.edu.cn; xudegang@tju.edu.cn; shiwei@tju.edu.cn; jqyao@tju.edu.cn).

J. Xu is with the Department of Electrical and Computer Engineering, The University of Texas at Austin, Austin, TX 78712 USA (e-mail: xujiamingnil@utexas.edu).

Color versions of one or more of the figures in this letter are available online at http://ieeexplore.ieee.org.

Digital Object Identifier 10.1109/LPT.2019.2942613

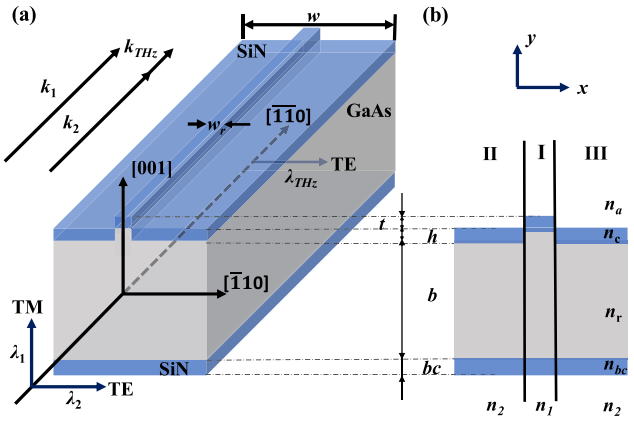

Fig. 1. The GaAs/SiN ridge waveguide structure. (a) Schematic diagram; (b) Waveguide cross-section.

bonded to a silicon wafer or an SOI platform [14], [15] which ensures an excellent compatibility. By using 2-μm and 10-μm lasers as the pump sources for waveguides with three different sizes, monochromatic terahertz waves in the 1.59–2.66 THz frequency range can be achieved. The highest output power is 56.16 μW, corresponding to conversion efficiency of $5.62 \times 10^{-5}\mathrm{W}^{-1}$, which are much higher than the previous works based on bulk and micro-structured GaAs crystals [3].

II. Details of the GaAs/SiN Hybrid Ridge Waveguide

The detailed schematic of the ridge waveguide is shown in Fig. 1 (a). The GaAs is grown along [001], and the waveguide is designed so that light propagates along the [$\bar{1}\bar{1}$0] direction to guarantee the largest nonlinear susceptibility for type-II DFG [16]. Available techniques to analyze waveguide structures include the effective index method (EIM), the finite difference method, and the function fitting method [17], [18]. All these methods are based on the premise of no E-field component along the propagation direction. As a semi-analytic algorithm, the EIM was originally proposed for calculating rectangular dielectric waveguides, and has been working as the most common method in the past few decades. The cross-section of the waveguide shown in Fig. 1(b) is divided into three parts—I, II, and III, where two side parts are identical for symmetry, and both the lateral side boundaries and the bottom substrate are infinite. For sections I and II, the effective refractive indices $n_i (i = 1, 2)$ can be calculated by [19], [20]

$$\frac{2\pi}{\lambda_0} L\sqrt{n_r^2 - n_i^2} = arctan\left[\left(\frac{n_r}{n_s}\right)^{2m}\sqrt{\frac{n_i^2 - n_{bc}^2}{n_r^2 - n_i^2}}\right] + arctan\left[\xi\frac{\psi cosh\varphi - sinh\varphi}{\psi cosh\varphi + sinh\varphi}\right] \quad (1)$$

where

$$\xi = \left(\frac{n_r}{n_c}\right)^{2m}\sqrt{\frac{n_i^2 - n_c^2}{n_r^2 - n_i^2}}$$

$$\psi = \left(\frac{n_c}{n_{bc}}\right)^{2m}\sqrt{\frac{n_i^2 - n_a^2}{n_i^2 - n_c^2}}$$

$$\varphi = \frac{2\pi}{\lambda_0} l\sqrt{n_i^2 - n_c^2}$$

TABLE I
Dimensions of the Ridge Waveguides

Sample	w_r(μm)	w(μm)	t (μm)	h(μm)	b(μm)	bc(μm)
G1	5	50	0.5	0.5	30	1
G2	5	50	1	1	30	1
G3	5	50	1	1	32	1

in which λ_0 is the vacuum wavelength, b, h, t and bc are the slab thickness, the ridge depth (the same as side cladding), the top cladding, and the bottom cladding, respectively, n_a, n_c, n_r and n_{bc} are the indices of air, the top cladding, the core waveguide, and the bottom cladding, respectively, m =0 and m =1 represent TE and TM polarizations, respectively. In section I, $L = b+h+t$ and $l = t$, while in section II, $L = b + h$ and $l = h$. The effective index of the ridge waveguide n_3 can be obtained by substituting n_i $(i = 1, 2)$ into

$$\frac{2\pi}{\lambda_0} w_r\sqrt{n_1^2 - n_2^2} = 2arctan\left[\left(\frac{n_1}{n_2}\right)^{2m}\sqrt{\frac{n_3^2 - n_2^2}{n_1^2 - n_2^2}}\right] \quad (2)$$

where w_r is the ridge width.

Three waveguides with different specifications are studied with their dimensions listed in Table 1. The ridge width is 5 μm and the ridge height is larger than 0.5 μm, which ensure not only the feasibility of lithography, but also the fabrication uniformity and reproducibility [18]. The waveguide can be fabricated by the following steps: firstly, a SiN bottom cladding is deposited onto a GaAs wafer by plasma enhanced chemical vapor deposition (PECVD) and the SiN side is heterogeneously bonded to a silicon wafer [14], [15]; then the GaAs wafer is wet chemical etched to the desired thickness, and the ridge structure is constructed by photolithography and reactive ion etching (RIE); after that, a SiN top cladding is deposited onto the waveguide. Before deposition during each step, chemical treatments should be applied to remove the native oxides of the GaAs wafers, and both sides of the waveguide need passivation to finish the fabrication [21].

III. Simulation Results and Discussions

The following PM condition for the DFG process in waveguides should be satisfied [6]:

$$(n_p\omega_p - n_s\omega_s)/(\omega_p - \omega_s) = n_g = n_{THz} \quad (3)$$

where ω_p and n_p are the angular frequency and effective refractive index of the TM-mode pump laser, while ω_s and n_s are the ones of the TE-mode pump laser. Only when the waveguide group refractive index n_g and the effective terahertz index n_{THz} are the same, the PM condition can be achieved. To avoid the strong two-photon absorption in GaAs, laser wavelengths around 2 μm and 10 μm are used as pump sources, which can be obtained via compact Tm^{3+}-doped fiber lasers and quantum cascade lasers (QCLs), respectively.

For terahertz generation pumped by 2-μm lasers, the relations between n_g and n_{THz} with three waveguides are shown in Fig. 2 (a). The TM-mode pump laser involved in the DFG process is fixed at 2.11 μm, and the TE-mode ones are tuned to 2.1503, 2.1498, and 2.1469 μm, respectively. The variation of n_g with both the waveguide size and generated terahertz frequency is inconspicuous, while n_{THz} has a significant dependence with terahertz frequency. The curves of

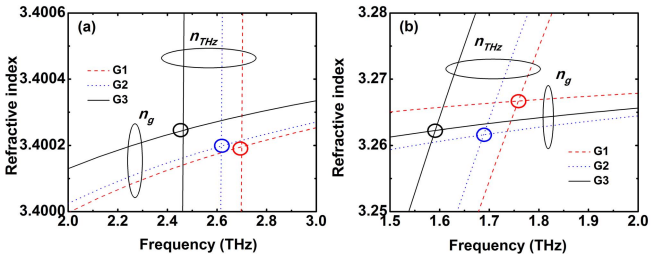

Fig. 2. Relations of the group refractive index (n_g) and the effective terahertz index (n_{THz}) in the waveguides: (a) pumping at 2 μm; (b) pumping at 10 μm.

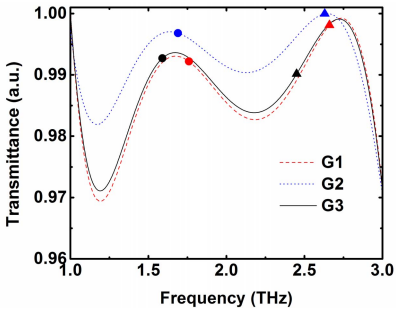

Fig. 3. Transmittance $|S_{21}|^2$ of the waveguides from 1 to 3 THz. The curves are transmissions through waveguides G1, G2, and G3, while the solid triangles and disks represent the terahertz waves with 2- and 10-μm pump lasers, respectively.

n_g and n_{THz} intersect at 2.66 THz (112.6 μm), 2.63 THz (113.9μm), and 2.45 THz (122.6 μm) for G1, G2, and G3, respectively. Thus, efficient DFG can be achieved at these frequencies by fulfilling the PM conditions. Figure 2 (b) demonstrates the case of pumping with 10-μm lasers, where the fixed TM-mode pump wavelength is at 9.8 μm, and the other TE-mode lasers are at around 10.40, 10.37, and 10.34 μm, respectively. In Fig. 2(b), the variation tendencies of n_g and n_{THz} are similar to those in Fig. 2(a), but the slopes are significantly higher for n_g. For three waveguides G1, G2 and G3, the intersections are located at 1.76 THz (170.6 μm), 1.69 THz (177.7 μm), and 1.59 THz (188.6 μm), respectively. From the above results, it can be concluded that 10-μm lasers give lower terahertz frequencies in the same waveguide. Furthermore, waveguides with larger ridge depths and thicknesses can achieve lower terahertz frequencies under the same pumping condition. The ridge depth, thickness, and pump wavelength are all flexible parameters for generating widely tunable monochromatic terahertz waves. However, the terahertz frequency is insensitive to the ridge width according to the calculations.

To ensure efficient outcoupling, the ridge waveguides should have high transmittance in the terahertz range. The Scattering-parameters (S-parameters), especially S_{21}, are usually used to analyze the transmission properties of waveguides [22]. Fig. 3 demonstrates the transmission $|S_{21}|^2$ curves of three waveguides G1, G2, and G3 from 1 to 3 THz, calculated by the CST Studio Suite. All the waveguides are assumed to be 15 mm in length and only the properties of the fundamental modes are considered. From the simulations, it is found that G2 has a relative larger $|S_{21}|$ than the other two. Two transmission peaks are located around 1.6 and 2.5 THz, mainly caused by intrinsic resonance of the waveguide structures and mesh density. The overall transmissions are beyond 0.96,

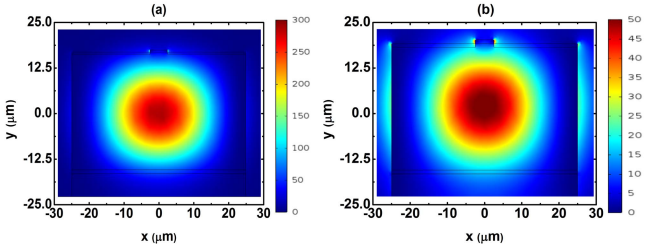

Fig. 4. Electric field distributions simulated for the TE-mode terahertz waves: (a) 2.66 THz (2-μm pumping in G1); (b) 1.59 THz (10-μm pumping in G3).

which is favorable for the output coupling efficiency of the terahertz waves generated in these ridge waveguides.

The typical distribution of the electric field for the ridge waveguide is calculated with COMSOL Multiphysics. Fig. 4 gives the two-dimensional (2D) electromagnetic simulations of the TE-mode terahertz waves at 2.66 (2-μm pumping in G1) and 1.59 THz (10-μm pumping in G3), by assuming that the waveguides are bonded on silicon substrates and the ambiance is air. Electric fields at both frequencies can be well confined in the waveguides (the one at 2.66 THz is confined better due to its smaller mode size) with Gaussian-like distributions.

Given that the input continuous-wave (CW) laser powers at two pump wavelengths were both 1 W ($P_1 = P_2 = 1$ W), the output terahertz power (P_{THz}) under PM condition is expected to follow [6], [23]

$$P_{THz} = \frac{1}{2} Z \frac{4\pi^2 \left(2d_{eff}\right)^2 L^2}{n_p n_s n_{THz} (\lambda_{THz})^2} \left(\frac{P_1 P_2}{S_{eff}}\right) \times e^{-\alpha_{THz} L} \frac{1 + e^{-\Delta\alpha L} - 2e^{-\frac{1}{2}\Delta\alpha L}}{\left(\frac{1}{2}\Delta\alpha L\right)^2} \quad (4)$$

where $Z = \sqrt{\mu_0/\varepsilon_0}$ is the impedance of free space, S_{eff} is the effective nonlinear interaction area, α_p, α_s, and α_{THz} are the power absorption coefficients at ω_p, ω_s, and ω_{THz}, respectively, $\Delta\alpha = \alpha_p + \alpha_s - \alpha_{THz}$, n_p, n_s, and n_{THz} are the effective refractive indices of the fundamental modes at ω_p, ω_s, and ω_{THz}, respectively, and L is the length of the waveguide. According to the Miller's rule [24], the effective nonlinear coefficients d_{eff} in the DFG process are estimated to be 182 and 150 pm/V [25], when pumped by the 2-μm and 10-μm lasers, respectively. The absorption coefficient of the 2-μm and 10-μm lasers in the waveguide are both 0.1 cm^{-1}. The absorption coefficients of terahertz waves from 2.45 to 2.66 THz are assumed to be the same of 4.5 cm^{-1}, and those at 1.59, 1.69, and 1.76 THz are 1.2, 1.5, and 2 cm^{-1}, respectively [9]. The effective interaction areas for 2-μm and 10-μm pumping are around 904.32 μm^2 and 1276.94 μm^2, respectively. Fig. 5 illustrates the terahertz power versus waveguide length with two different pumping bands. When the waveguide length is around 14.5 mm, the highest terahertz output power of 34.11 μW can be achieved at 2.66 THz pumped by 2-μm lasers in G1, as shown in Fig. 5(a). The corresponding conversion efficiency is 3.41×10^{-5}W^{-1}. Since the output power is inversely proportional to the squared wavelength (given that the other conditions are the same), the output powers from G2 and G3 should be lower compared with that from G1, which agrees well with the results of Fig. 5 (a). However, it is a different case shown in Fig. 5 (b),

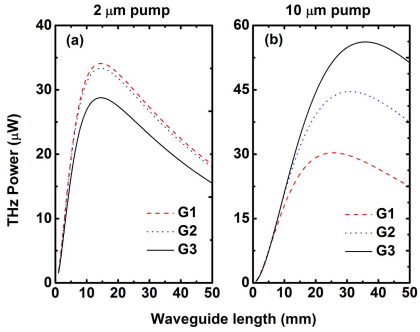

Fig. 5. Terahertz output powers calculated from Eq. (4) versus the waveguide lengths. (a) and (b) are the results using 2-μm and 10-μm pump lasers, respectively.

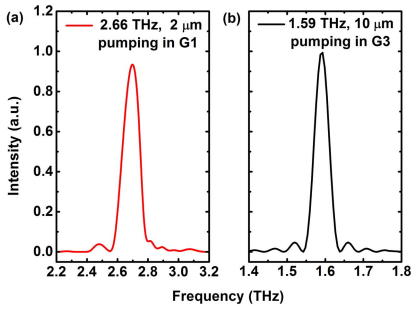

Fig. 6. Simulated terahertz output spectra: (a) 2.66 THz (2-μm pumping in G1); (b) 1.59 THz (10-μm pumping in G3).

where longer waveguides are required for maximum output power, and the terahertz absorption coefficient increases with frequency. Attributing to smaller absorption coefficients, the maximum terahertz output power is 56.16 μW at 1.59 THz with 10-μm laser pumping in G3, corresponding to a DFG efficiency of 5.62×10^{-5} W^{-1}, which is much higher than a previously reported result of 1.24×10^{-6} W^{-1} based on a bulk GaAs crystal [3]. Output spectra at 2.66 (2-μm pumping in G1) and 1.59 THz (10-μm pumping in G3) are shown in Fig. 6, where the 3 dB linewidths are around 0.1 and 0.05 THz, respectively, calculated by slightly tuning the pump wavelength to vary the phase mismatch Δk, since the output power is proportional to $sinc^2(\Delta kL/2)$.

IV. Conclusion

In this paper, a flexible ridge waveguide structure based on GaAs and SiN, which can be fabricated with standard clean-room equipment, is proposed to generate terahertz waves via DFG. By using pump lasers around 2 μm and 10 μm, CW terahertz waves from 1.59 to 2.66 THz could be achieved with the maximum output power of 56.16 μW at 1.59 THz, corresponding to a DFG conversion efficiency of 5.62×10^{-5} W^{-1}. Wavelength tuning is accessible by changing the ridge depth and thickness of the waveguides. Comparing with previous reports using bulk GaAs crystals in generating terahertz waves, such a waveguide structure can realize much higher conversion efficiency, and demonstrate great potential in on-chip terahertz systems by bonding it to a silicon wafer or integrated platforms.

References

[1] D. Dragoman and M. Dragoman, "Terahertz fields and applications," *Prog. Quantum Electron.*, vol. 28, no. 1, pp. 1–66, Jan. 2004.
[2] M. Tonouchi, "Cutting-edge terahertz technology," *Nature Photon.*, vol. 1, no. 2, pp. 97–105, 2007.
[3] J. Mei *et al.*, "High-repetition-rate terahertz generation in QPM GaAs with a compact efficient 2-μm KTP OPO," *IEEE Photon. Technol. Lett.*, vol. 28, no. 14, pp. 1501–1504, Jul. 15, 2016.
[4] K. Zhong *et al.*, "Optically pumped terahertz sources," *Sci. China Technol. Sci.*, vol. 60, no. 12, pp. 1801–1818, Dec. 2017.
[5] R. S. Jacobsen *et al.*, "Strained silicon as a new electro-optic material," *Nature*, vol. 441, pp. 199–202, May 2006.
[6] K. Saito, T. Tanabe, and Y. Oyama, "THz-wave generation via difference frequency mixing in strained silicon based waveguide utilizing its second order susceptibility $\chi^{(2)}$," *Opt. Express*, vol. 22, no. 14, pp. 16660–16668, Jul. 2014.
[7] K. Saito, T. Tanabe, and Y. Oyama, "Design of a GaP/Si composite waveguide for CW terahertz wave generation via difference frequency mixing," *Appl. Opt.*, vol. 53, no. 17, pp. 3587–3592, Jun. 2014.
[8] S. Fan, H. Takeuchi, T. Ouchi, K. Takeya, and K. Kawase, "Broadband terahertz wave generation from a MgO:$LiNbO_3$ ridge waveguide pumped by a 1.5 μm femtosecond fiber laser," *Opt. Lett.*, vol. 38, no. 10, pp. 1654–1656, May 2013.
[9] K. L. Vodopyanov, "Optical THz-wave generation with periodically-inverted GaAs," *Laser Photon. Rev.*, vol. 2, nos. 1–2, pp. 11–25, Jan. 2008.
[10] D. B. Anderson and J. T. Boyd, "Wideband CO_2 laser second harmonic generation phase matched in GaAs thin-film waveguides," *Appl. Phys. Lett.*, vol. 19, no. 8, pp. 266–268, Oct. 1971.
[11] D. E. Thompson and P. Coleman, "Step-tunable far infrared radiation by phase matched mixing in planar-dielectric waveguides," *IEEE Trans. Microw. Theory Techn.*, vol. MTT-22, no. 12, pp. 995–1000, Dec. 1974.
[12] A. Marandi, T. E. Darcie, and P. P. M. So, "Design of a continuous-wave tunable terahertz source using waveguide-phase-matched GaAs," *Opt. Express*, vol. 16, no. 14, pp. 10427–10433, Jul. 2008.
[13] K. Saito, T. Tanabe, and Y. Oyama, "Design of an efficient terahertz wave source from a GaP waveguide embedded in a silicon slot waveguide," *J. Eur. Opt. Soc.-Rapid Publications*, vol. 10, pp. 1–6, May 2015.
[14] S. Sánchez, C. Gui, and M. Elwenspoek, "Spontaneous direct bonding of thick silicon nitride," *J. Micromech. Microeng.*, vol. 7, no. 3, pp. 111–113, Apr. 1997.
[15] L. Chang *et al.*, "Heterogeneously integrated GaAs waveguides on insulator for efficient frequency conversion," *Laser Photon. Rev.*, vol. 12, no. 10, Aug. 2018, Art. no. 1800149.
[16] P. S. Kuo *et al.*, "GaAs optical parametric oscillator with circularly polarized and depolarized pump," *Opt. Lett.*, vol. 32, no. 18, pp. 2735–2737, Sep. 2007.
[17] J. Buus, "The effective index method and its application to semiconductor lasers," *IEEE J. Quantum Electron.*, vol. QE-18, no. 7, pp. 1083–1089, Jul. 1982.
[18] M. J. Robertson, S. Ritchie, and P. Dayan, "Semiconductor waveguides: Analysis of optical propagation in single rib structures and directional couplers," *IEE Proc. J.-Optoelectron.*, vol. 132, no. 6, pp. 336–342, Dec. 1985.
[19] K. S. Chiang, "Effective-index analysis of optical waveguides," *Proc. SPIE*, vol. 2399, pp. 1–12, Jun. 1995.
[20] C. Tyszkiewicz, "Homogeneous sensitivity of sol-gel derived planar waveguide structures—Theoretical analysis," *Opt. Appl.*, vol. 42, no. 3, pp. 555–569, Jan. 2012.
[21] M. Rebaud, M.-C. Roure, V. Loup, P. Rodriguez, E. Martinez, and P. Besson, "Chemical treatments for native oxides removal of GaAs wafers," *ECS Trans.*, vol. 69, no. 8, pp. 243–250, Oct. 2015.
[22] R. Yan, B. Sensale-Rodriguez, L. Liu, D. Jena, and H. G. Xing, "A new class of electrically tunable metamaterial terahertz modulators," *Opt. Express*, vol. 20, no. 27, pp. 28664–28671, Dec. 2012.
[23] R. L. Aggarwal and B. Lax, *Nonlinear Infrared Generation*, Y. R. Shen, Ed. New York, NY, USA: Springer-Verlag, 1977, pp. 28–29.
[24] R. C. Miller, "Optical second harmonic generation in piezoelectric crystals," *Appl. Phys. Lett.*, vol. 5, no. 1, pp. 17–19, Nov. 1964.
[25] M. M. Choy and R. L. Byer, "Accurate second-order susceptibility measurements of visible and infrared nonlinear crystals," *Phys. Rev. B, Condens. Matter*, vol. 14, no. 4, pp. 1693–1706, Aug. 1976.